Variable Rate Neural Compression for Sparse Detector Data

Yi Huang[a], Yeonju Go[a], Jin Huang[a], Shuhang Li[c], Xihaier Luo[a], Thomas Marshall[e], Joseph D. Osborn[a], Christopher Pinkenburg[a], Yihui Ren[a], Evgeny Shulga[a,d], Shinjae Yoo[a], Byung-Jun Yoon[a,b]

[a]*Brookhaven National Laboratory, PO Box 5000, Upton, NY, 11973, USA*
[b]*Texas A&M University, 3128 TAMU, College Station, TX, 77843, USA*
[c]*Columbia University, 538 West 120th Street, New York, NY, 10027, USA*
[d]*Stony Brook University, 100 Nichols Road, Stony Brook, NY, 11794, USA*
[e]*University of California, Los Angeles, 475 Portola Plaza, Los Angeles, CA, 90095, USA*

Abstract

High-energy large-scale particle colliders generate data at extraordinary rates, reaching up to one terabyte per second in nuclear physics and several petabytes per second in high-energy physics. Developing real-time high-throughput data compression algorithms to reduce data volume and meet the bandwidth requirement for storage has become increasingly critical. Deep learning is a promising technology that can address this challenging topic. At the newly constructed sPHENIX experiment at the Relativistic Heavy Ion Collider, a Time Projection Chamber (TPC) serves as the main tracking detector, which records three-dimensional particle trajectories in a volume of a gas-filled cylinder. In terms of occupancy, the resulting data flow can be very sparse reaching 10^{-3} for proton-proton collisions. Such sparsity presents a challenge to conventional learning-free lossy compression algorithms, such as SZ, ZFP, and MGARD. In contrast, emerging deep learning-based models, particularly those utilizing convolutional neural networks for compression,

have outperformed these conventional methods in terms of compression ratios and reconstruction accuracy. However, research on the efficacy of these deep learning models in handling sparse datasets, like those produced in particle colliders, remains limited. Furthermore, most deep learning models do not adapt their processing speeds to data sparsity, which affects efficiency. To address this issue, we propose a novel approach for TPC data compression via *key-point identification* facilitated by *sparse convolution*. Our proposed algorithm, `BCAE-VS`, achieves a 75% improvement in reconstruction accuracy with a 10% increase in compression ratio over the previous state-of-the-art model. Additionally, `BCAE-VS` manages to achieve these results with a model size over two orders of magnitude smaller. Lastly, we have experimentally verified that as sparsity increases, so does the model's throughput. Our code along with the pretrained models and dataset used for model development are available at `https://github.com/BNL-DAQ-LDRD/NeuralCompression_v3` and `https://zenodo.org/records/10028587`, respectively.

Keywords: Deep Learning, Autoencoder, High-throughput Inference, Data Compression, Sparse Data, Sparse Neural Network, High Energy and Nuclear Physics

1. Introduction

1.1. Background

High-energy particle colliders, such as the Large Hadron Collider (LHC) [1] and the Relativistic Heavy Ion Collider (RHIC) [2], are critical tools for probing the fundamental building blocks of matter. In these experiments, protons and heavy ions are accelerated to velocities approaching the speed of
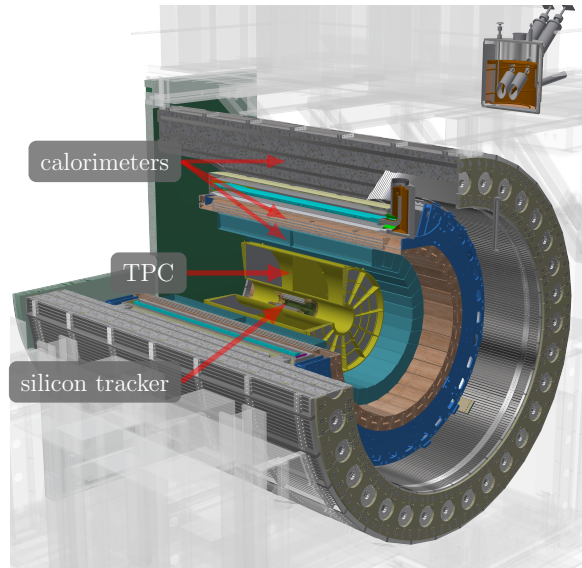
Figure 1: **sPHENIX detector assembly. Time projection chamber (TPC) contributes the majority of data.**

light and providing collisions at extremely high energies (for RHIC nucleon-nucleon center of mass energy is $200\,\text{GeV}$ in heavy ion collisions up to and $510\,\text{GeV}$ in proton-proton collisions). These complex interactions generate a multitude of subatomic particles (thousands of particles in the central heavy ion collisions), enabling scientists to explore the deepest questions about the nature of the universe. To capture the products of collisions, the interaction point is surrounded by the state of art particle detectors. Recently constructed sPHENIX experiment [2] at RHIC focuses on studying the microscopic properties of strongly interacting matter, such as the quark-gluon plasma, a state of matter that existed in the early universe.

To achieve this, sPHENIX employs an array of advanced particle detectors (Figure 1). The Time Projection Chamber (TPC) [3] is the primary tracking detector. The TPC acts as a three-dimensional (3D) camcorder, continu-

ously recording the trajectories of charged particles as they pass through its detection volume. As particles move through the TPC, they ionize the gas molecules, creating clusters of charge. Clusters drift in the electric field to the readout pads and induce electrical signals. These signals (hits) are registered by 160 thousand detector channels. Both the position and time of a hit are captured by one of the 40 million voxels in a 3D grid of the active detection volume. The system then digitizes these signals, transforming them into analog-to-digital conversion (ADC) values. The TPC readout digitizes 3.2 trillion voxels per second and generates terabits per second of data after zero suppression.

Traditionally, collider experiments have relied on a level-1 trigger system to manage the massive data output by selecting only the most significant collision events for storage, while discarding less valuable data. However, next-generation collider experiments, including sPHENIX, are moving towards streaming data acquisition (DAQ) systems [4, 5, 6], which aim to continuously record a large fraction to *all* collision events. While this approach maximizes the physics output, it presents a critical challenge: handling the immense data volume in real time.

To reduce the TPC data volume while preserving key information, efficient data compression techniques are essential. This paper introduces a deep neural network-based lossy compression algorithm designed to meet the high-throughput demands of streaming DAQ systems. Moreover, unlike specialized algorithms tailored specifically for TPC data [7], our approach is *data-driven* and makes no assumptions about the underlying physics, allowing it to generalize to other datasets with similar characteristics, such as

those for the future electron-ion collider [6, 5].

1.2. Related Work and Research Gaps

Conventional scientific lossy compression methods are motivated in fields such as climate science, fluid dynamics, cosmology, and molecular dynamics. These methods have been driven by the necessity to handle large datasets produced by distributed and high-fidelity simulations in a high-performance computing environment. For example, the error-bounded SZ compression algorithm [8, 9, 10] has proven effective for compressing data from climate science and cosmology simulations. Other examples include the ZFP method [11], which was developed specifically for hydrodynamics simulations, and the MGARD method [12, 13], which was designed to compress turbulent channel flow and climate simulation data.

While there is extensive research on general-purpose lossy compression, few existing methods are optimized for highly sparse data. Although the aforementioned compression algorithms have demonstrated reasonable performance with TPC data, none of them are specifically tailored for this type of input. In this context, a specialized neural network-based compression model, the *Bicephalous Convolutional Auto-Encoder* (`BCAE`), introduced in [14] and later refined in [15], has been shown to outperform traditional methods in terms of both compression ratio and reconstruction accuracy for sparse TPC data.

However, despite the `BCAE`'s superior performance, its design treats the sparsity of TPC data as a challenge to overcome rather than as an opportunity to improve compression efficiency. The `BCAE` model compresses data by mapping the input array to a *fixed-size* code, regardless of the input's

occupancy (i.e., the fraction of non-zero elements). This results in ineffi-ciencies: when the code size is large enough to accommodate inputs with high signal occupancy, there is wasted space for sparser inputs; conversely, when the code size is optimized for sparser inputs, denser inputs suffer from information loss during compression.

1.3. Challenges and Solutions

Challenge 1. Occupancy-based variable compression ratio. While TPC data on average exhibits low occupancy (around 10%), the actual oc-cupancy can vary significantly. For instance, in the dataset used for model development, occupancy ranges from less than 5% to over 25%. Therefore, there is a need for compression algorithms capable of producing larger codes for denser inputs and smaller codes for sparser ones.

Solution. We propose `BCAE-VS`, a bicephalous autoencoder that provides a variable compression ratio based on TPC data occupancy. The design of `BCAE-VS` is motivated by the hypothesis that a trajectory can be reliably reconstructed from a subset of signals. Consequently, *data compression can be achieved by selectively down-sampling signals rather than resizing the input array.* To implement this, `BCAE-VS`'s encoder predicts the importance of each signal in the input array for trajectory reconstruction. Signals with higher importance are treated as analogous to the *key points* that anchor shapes in computer vision tasks such as action and gesture recognition [16, 17, 18, 19]. Compression is achieved by saving only the coordinates and neural representations of these key points.

Challenge 2. Leveraging sparsity for throughput. Despite the im-pressive reconstruction accuracy of `BCAE-VS`, implementing its encoder with

6

conventional (dense) convolution operations will lead to constant computation time disregarding input data with changing sparsity and complexity.

Solution. We use *sparse convolution* for implementing BCAE-VS's encoder. With a manageable runtime overhead, the sparse convolution-powered encoder of BCAE-VS generates output only for the signals with input exclusively from the signals and skips all matrix multiplications with all-zero operands. As the overhead and the number of non-zero values vary with occupancy, BCAE-VS achieves a variable throughput that increases significantly as occupancy decreases.

Main Contributions:

- **Introduction of BCAE-VS:** We propose BCAE-VS, an improved BCAE model enabling Variable compression ratio for Sparse data. This model aims to enhance both compression efficiency and reconstruction accuracy by selectively down-sampling signals rather than reducing the size of the input array.

- **Improved reconstruction performance:** BCAE-VS achieves a 75% improvement in reconstruction accuracy and a 10% higher compression ratio on average compared to the most accurate BCAE model.

- **Use of sparse convolution for high throughput:** To address the computational inefficiencies of conventional convolution with high sparsity data, BCAE-VS employs sparse convolution. This approach processes only the relevant signals, significantly reducing the computational overhead associated with matrix multiplications involving all-zero operands.

2. TPC Data

2.1. Overview

Figure 2 shows a schematic view of sPHENIX TPC. sPHENIX TPC is a cylindrical gas-filled drift chamber. Working gas mixture is 75% argon (Ar), 20% carbon tetrafluoride (CF_4), and 5% isobutane (C_4H_{10}). Collisions happen in the center of the TPC. Charged particles produced in the collisions traverse the volume of the TPC at a speed close to the speed of light. As charged particles travel, they ionize the gas atoms along trajectories and create trails of electrons and ions. Extremely uniform electric field $E = 400\,V\,cm^{-1}$ provides uniform drift velocity for electron clouds drift towards the readout planes. The positions and arrival times of the electrons are recorded by the sensors arranged in concentric layers on the readout planes. Gas ionization by a particle depends only on its velocity and the square of the charge, thus the density of the electron cloud allows to distinguish different particles, e.g. protons, kaons, and pions. The chamber is placed within the magnetic field of a superconducting magnet, which provides a magnetic field $B = 1.4\,T$ collinear with the electric field. Trajectory of the particle is bent by the magnetic field along the axial direction. This bending allows for the determination of the momenta and charges of the particles based on the curvature of their trajectory.

The sPHENIX TPC readout plane has three groups of layers: inner, middle, and outer. Each layer group produces a readout of a 3D (axial, radial, and azimuthal) array of ADC values. Each array has 16 layers along the radial direction and 249 temporal sampling points (for one TPC drift time window) along the axial direction on each side of the TPC, representing
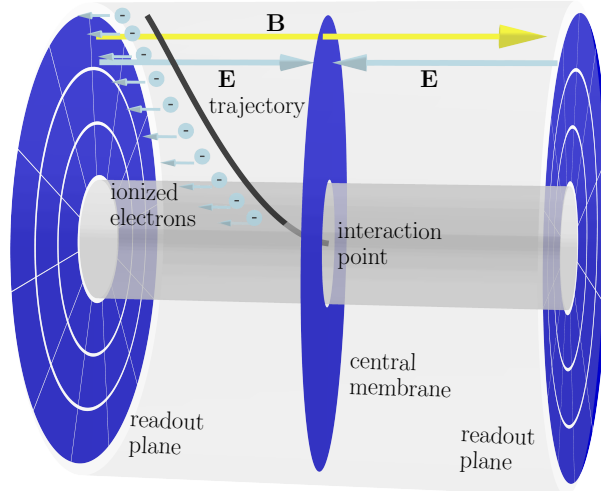
Figure 2: **A schematic view of sPHENIX TPC.**

time evolution. The number of readout pads along the azimuthal direction increases from inner to outer layers. The number is constant within a layer group and it is 1152, 1536, and 2304, respectively. In this study, we will focus on the 16 layers of the outer group of the TPC with 2304 readout pads along the azimuthal direction. Each element in the (layer, pad, temporal) array is mapped to a *voxel* in the 3D space. We demonstrate a full azimuthal outer layer group readout in Figure 3A (experiment 3060, event 8 in the test split of the dataset).

To match the subdivision of the readout electronics in the TPC readout chain, the data from a layer group has the same division. It has 24 equal-size non-overlapping sections: 12 along the azimuthal direction (30 degrees per section) and 2 along the axial direction (separated by the transverse plane passing the collision point). We call these sections *TPC wedges*. Figure 3B shows a zoom-in view of one of the wedges from the outer layer group. Each
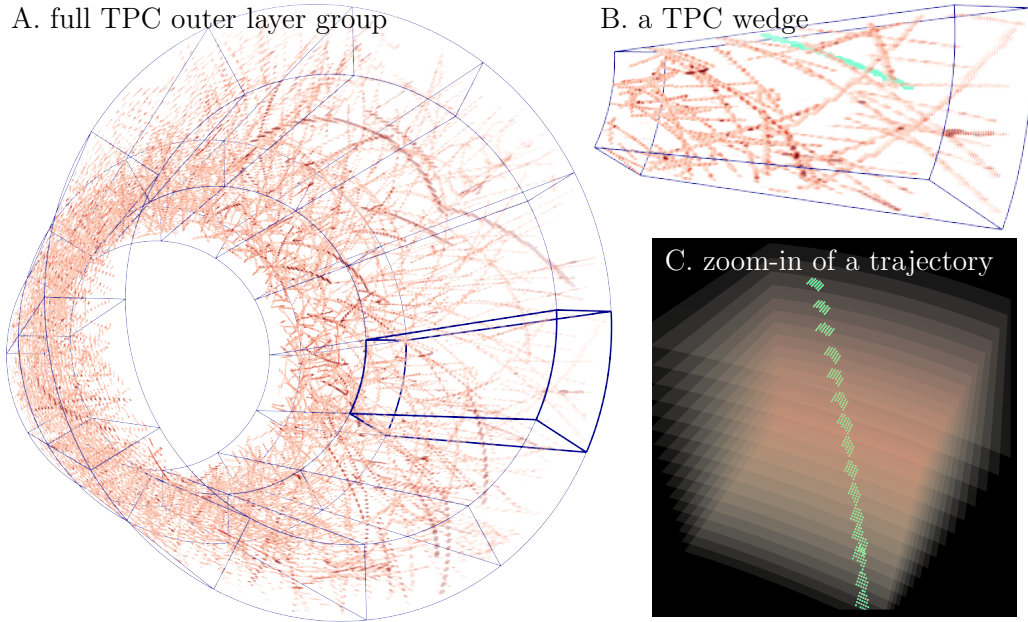
A. full TPC outer layer group

B. a TPC wedge

C. zoom-in of a trajectory

Figure 3: **Visualization of the outer layer group TPC data of an Au+Au collision event with** 0-10% **centrality and** 170 kHz **pileup.**

outer-layer wedge is an array of dimensions 16, 192, and 249 in radial, azimuthal, and axial directions, respectively. All ADC data from the same wedge will be transmitted to the same group of front-end electronics, after which a real-time lossy compression algorithm could be deployed. Therefore, TPC wedges are used as the direct input to the deep neural network compression algorithms.

2.2. Dataset and Preprocessing

To train a compression algorithm, we used a dataset containing 1310 simulated events for central $\sqrt{s_{\mathrm{NN}}} = 200$ GeV Au+Au collisions with 170 kHz pileup collisions[1]. The data were generated with the HIJING event genera-

---

[1]Zenodo linked: `https://zenodo.org/records/10028587`

tor [20] and Geant4 Monte Carlo detector simulation package [21] integrated with the sPHENIX software framework [22].

The simulated TPC readout (ADC values) from these events are represented as 10-bit unsigned integers $\in [0, 1023]$. To reduce unnecessary data transmission, a *zero-suppression* algorithm has been applied. All ADC values below 64 are set to be zero as large fraction of them represent noise. This zero-compression makes the TPC data sparse at about 10.8% occupancy of non-zero values. A voxel that has a non-zero ADC value is a *signal voxel*. A voxel with a 0 ADC value is a *non-signal voxel*.

We divide the 1310 total events into 1048 events for training and 262 for testing. Each event contains 24 outer-layer wedges. Thus, the training partition contains 25152 TPC outer-layer wedges, while the testing portion has 6288.

Finally, as trajectory coordinates must be interpolated from neighboring sensors using the ADC values, it is important to preserve the relative ADC ratio between the sensors. Hence, for this study, we work with *log ADC values* (defined as $\log_2(\text{ADC} + 1)$) instead of the raw ADC values. A log ADC value is a float number $\in [0., 10.]$. As zero-suppression is implemented at 64 for this dataset, and all nonzero log-ADC values exceed 6. Zero-suppression makes the distribution of ADC bimodal and extremely skewed.

Remark: This distribution presents a significant challenge for neural network-based algorithms since neural network tends to work well when input data is distributed approximately normally [23, 24]. In Section 3.1 we will show one approach to handle the discontinuity in the data distribution with a compression autoencoder equipped with two collaborating decoders. We

will discuss the limitation of this approach and provide a better solution in Section 3.2 with sparse convolution. As a result, the sparsity of the data is no longer an obstacle to overcome but rather an advantage that we can leverage.

3. Method

3.1. Bicephalous Convolutional Autoencoder

To address the problem caused by the difficult distribution of log ADC value, Bicephalous Convolutional Autoencoder (`BCAE`) was proposed in [14] and later optimized in [15]. A `BCAE` is an autoencoder with two decoders – one for segmentation and the other for regression (See Figure 4). During training, a code significantly smaller than the input is generated by the encoder and fed to the decoders. The segmentation decoder, D_{seg}, will output a score $s \in (0, 1)$ for each voxel in the input. The weights of D_{seg} are updated by comparing s to the true label of the input – 1 for a signal voxel and 0 for a non-signal voxel. The regression decoder, D_{reg}, will output a value r for each voxel. Given a threshold $s_0 \in (0, 1)$, the predicted value ($\hat{r}$) at each voxel is set to r if $s > s_0$ and to 0 if otherwise. The weights of D_{reg} are then updated by comparing $\hat{r}$ to the true input value of the voxel. The weights of the encoder E are updated with the combined gradient information from both decoders. During inference, we only run the encoder part and save the code to storage for later use.

The design of `BCAE` is motivated by two considerations: reconstruction accuracy and efficiency. First, the segmentation decoder is tasked to tackle the discontinuity in the input data distribution so that the regression decoder

12

can focus solely on approximating the ADC values. Second, having two decoders does not affect the compression (inference) throughput as only the encoder will be executed during compression. From the first consideration, we can see that a better solution with respect to reconstruction accuracy might be to have two single-tasking encoder-decoder pairs. However, since the encoding will run in real-time in deployment, it is crucial to keep the encoder simple and lightweight as much as possible for the high TPC data rate. Additionally, as demonstrated in [15], the possible adverse effect of a simple encoder could be compensated to some extent by a more complicated decoder.
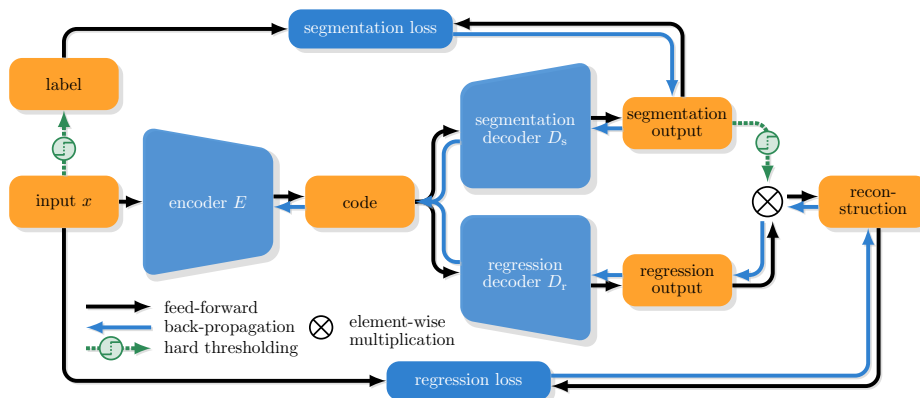

Figure 4: **Bicephalous convolutional autoencoder**.

Although BCAE has been shown to outperform existing non-neural network-based compression algorithms in reconstruction accuracy at equal or higher compression ratio [14], the approach does not leverage the sparsity of the input. First, its dense convolution incurs static computation costs despite varying input sparsity. Second, to produce a significantly smaller code, the down-sizing in the encoder breaks the sparsity of the input. This makes it

hard for the decoders to reconstruct a trajectory at its correct location, especially in higher occupancy areas (see Figure 10). Finally, for BCAE, the same code length is used regardless of data sparsity. This means that if a chosen code length is suitable for sparse and relatively simple data, it will become insufficient for denser and more complex ones.

3.2. BCAE-VS for Key-Point Identification

Figure 3C shows a close-up view of a typical trajectory formed by a streak of signal patches. The localized and seemingly redundant signal voxels of the same patch suggest the possibility of reconstructing the trajectory with only a fraction of them. As a starter, we performed a sanity check by randomly masking out 50% of signal voxels and used a neural network to reconstruct the original input. This compression by random sampling does not even require a learnable encoder network! The reconstruction mean squared error (MSE) (in raw ADC) is 95, which is much smaller than the 218 reported in [14].

These results suggest that if randomly selected signal voxels can perform effectively in reconstruction, a carefully *selected* subset of signal voxels should yield even better performance. Such a subset is analogous to the *key points* in computer vision, to which location a geometric shape is anchored. This concept led to the development of BCAE-VS whose encoder *compresses by down-selecting signal voxels rather than down-sizing the whole input array.*
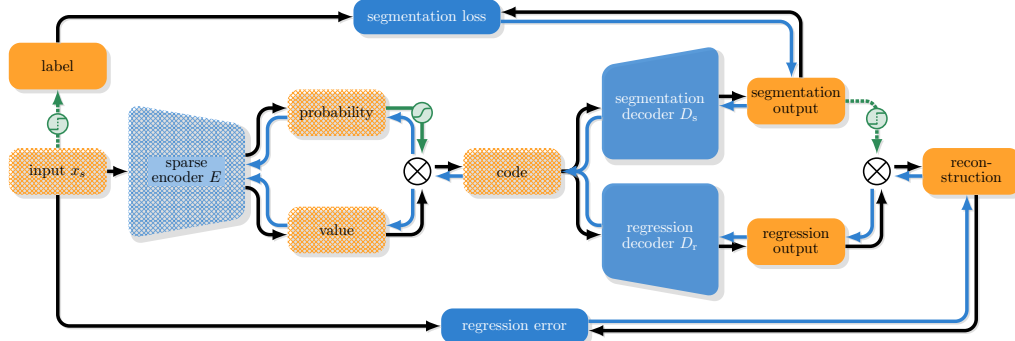
To achieve compression by down-selecting, an encoder assigns an importance score to each signal voxel, retaining only those with higher importance and discarding the rest. However, implementing such an encoder with standard (dense) convolutions requires running 3D convolutions that maintain

the input dimension, which can be relatively slow [15]. This is where *sparse convolution* becomes a potentially better alternative, as it can compute solely for the signal voxels and use input exclusively from them.

This section is structured as follows: Section 3.2.1 explains the operation of `BCAE-VS`. Section 3.2.2 contrasts sparse convolution with dense convolution. In Section 3.2.3, we explore using random thresholding for identifying key signal voxels. Finally, Section 3.2.4 addresses the balance between compression and reconstruction in `BCAE-VS`.

3.2.1. The Working of BCAE-VS

A. `BCAE-VS` training
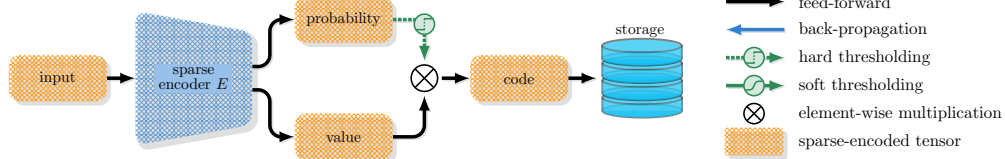

B. `BCAE-VS` inference

Figure 5: **Bicephalous autoencoder with sparse encoder for key-points identification.**

To describe `BCAE-VS` in more detail, let us first fix some notations. We will use x to denote a n-dimensional array and x_s to denote the sparse form of x with only the location and value of the non-zero entries specified. Although

x and x_s represent the same input, the different notations emphasize the fact that zeros (non-signal voxels) do not occupy any space in x_s while x contains all the zeros.

As demonstrated in Figure 5, for each entry in a TPC wedge x_s, the encoder E of `BCAE-VS` produces two outputs, importance score p and value v. The importance score output helps us determine the contribution of signal voxel in accurate reconstruction and the value is what we will save to the storage should the voxel be selected. There are two reasons for letting E produce v instead of using the original (raw or log) ADC value for reconstruction (as we did in the "encoder-free" compression). First, since we will have to save a value for a selected voxel anyway, an adjusted value produced by a trained neural network may be more helpful than the original (raw or log) ADC value. Second, the gain in inference speed from having one less output channel is marginal according to our experiment (at least for the specific sparse convolution implementation we chose for this work).

During the training of `BCAE-VS`, we pass importance score p through a soft mask function with an element-wise random threshold to get a soft mask m. The element-wise multiplication of v and m form the input to the decoders. For inference (compression only), the random soft thresholding will be replaced by a random hard thresholding. More details on the soft mask and random thresholding will be discussed in Section 3.2.

3.2.2. Sparse Convolution

For symbolic simplicity, we explain sparse convolution with input with two spatial dimensions, height and width. Generalization to a higher dimensional input is straightforward. We use s and d to denote the stride and

dilation of a convolution, and K_h and K_w to denote the kernel window for the height and width direction, respectively. For example, for convolution with kernel size 3, we have $K_\mathrm{h} = K_\mathrm{w} = [-1, 0, 1]$. We use i, o, h, w, k_h, and k_w to iterate through the input and output channels, height and width, and the kernel, respectively. The output Y can be calculated from the weight W, bias $\mathbf{b}$, and input X as follows:

$$
\begin{aligned}
Y_{o,h,w} &= \sum_{i,k_\mathrm{h},k_\mathrm{w}} W_{o,i,k_\mathrm{h},k_\mathrm{w}} X_{i,\,sh+dk_\mathrm{h},\,sw+dk_\mathrm{w}} + \mathbf{b}_o \\
&= \sum_{k_\mathrm{h},k_\mathrm{w}} \underbrace{\sum_{i} W_{o,i,k_\mathrm{h},k_\mathrm{w}} X_{i,\,sh+dk_\mathrm{h},\,sw+dk_\mathrm{w}}}_{\text{matrix multiplication}} + \mathbf{b}_o
\end{aligned}
\tag{1}
$$

For a dense convolution, the summation $\sum_{k_\mathrm{h},k_\mathrm{w}}$ is taken over $\mathcal{K} = K_\mathrm{h} \times K_\mathrm{w}$ and hence we cannot avoid the matrix multiplication in Equation 1 even if the input vector $X_{i,\,sh+dk_\mathrm{h},\,sw+dk_\mathrm{w}}$ is an all-zero vector. However, for a sparse convolution, the summation is taken over

$$
\mathcal{K}_{h,w} = \{(k_\mathrm{h}, k_\mathrm{w}) \,|\, (sh + dk_\mathrm{h},\, sw + dk_\mathrm{w}) \in \mathcal{S}\} \subset \mathcal{K}
$$

where $\mathcal{S}$ is the collection of coordinates in a sparse input. The map $(h, w) \mapsto \mathcal{K}_{h,w}$ is commonly referred to as the *kernel map* in the sparse convolution literature.

There are two types of sparse convolution: normal and submanifold sparse convolution. Let $\mathcal{N}_{h,w} = \{(sh + dk_\mathrm{h},\, sw + dk_\mathrm{w}) \,|\, (k_\mathrm{h}, k_\mathrm{w}) \in \mathcal{K}\}$ be the neighborhood of (h, w) with respect to the kernel, normal sparse convolution computes for a coordinate (h, w) if $\mathcal{N}_{h,w} \cap \mathcal{S}$ is not empty, while submanifold

sparse convolution only computes for $(h, w) \in \mathcal{S}$. Since normal sparse convolution will introduce new entries to $\mathcal{S}$ every time the convolution with kernel size > 1 is applied, and breaks the sparsity, we use *submanifold sparse convolution* for the `BCAE-VS` encoder.

As we can see from the discussion above, while sparse convolution can reduce runtime by avoiding computations on zero input, it incurs overhead from computing kernel maps. Consequently, sparse convolution is more efficient at lower sparsity but loses its advantage as sparsity decreases. Additionally, the efficiency of sparse convolution varies with the specific implementation. For this work, we use the `MinkowskiEngine` library from NVIDIA[2], as it provides the highest throughput on the hardware used in this research. Details on throughput are available in Section 4.3.
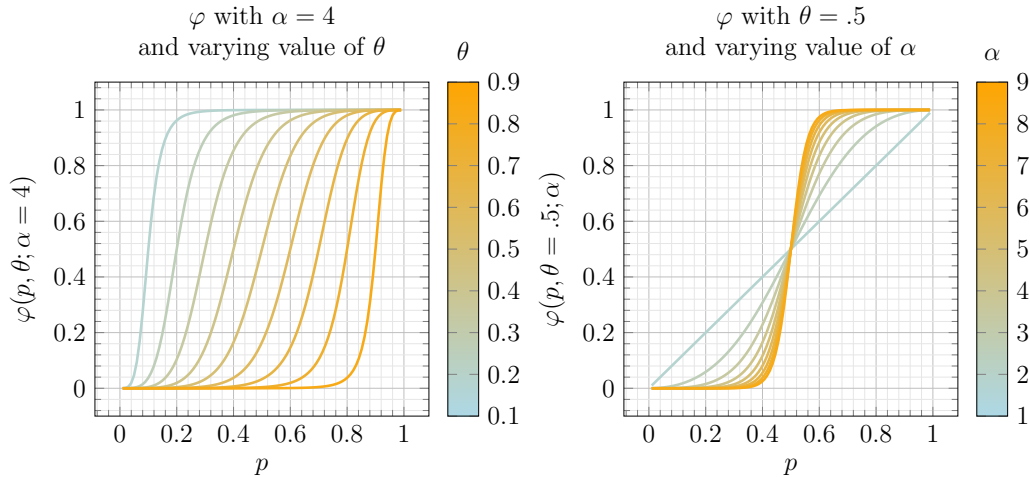
3.2.3. Random Thresholding
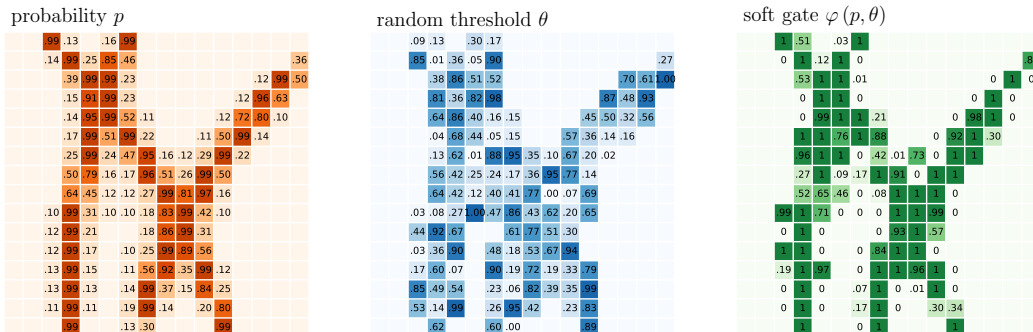

Figure 6: **The soft mask function.**

---

[2]`https://github.com/NVIDIA/MinkowskiEngine`

Figure 7: **Random thresholding.** For each signal voxel, the encoder will calculate an importance score p (left). A threshold θ is then generated following $\texttt{Uniform}(0,1)$ for each voxel (middle). A soft mask is obtained by $\varphi(p,\theta)$ (right).

The problem of key-point identification in TPC data compression can be thought of as a "self-supervised classification" problem. It is a classification problem since we want to predict a label 1 for a signal voxel crucial for accurate reconstruction and a 0 for a non-essential one. It is a self-supervised problem since we do not have a ground truth label to match but have to infer the label by observing the effect of keeping or discarding a signal voxel on reconstruction.

For this goal, we designed the random thresholding approach that works as follows. For a signal voxel with predicted importance score p, we generate a random number $\theta \sim \texttt{Uniform}(0,1)$, and calculate a soft mask with the function defined in Equation 2

$$\varphi(p,\theta;\alpha,\varepsilon) = \texttt{sigmoid}\left(\alpha\left[\texttt{logit}(p,\varepsilon) - \texttt{logit}(\theta,\varepsilon)\right]\right) \qquad (2)$$

The ε in the $\texttt{logit}$ function is used to improve numerical stability (p or $1-p$ less than ε will be replaced with ε). We set $\varepsilon = 10^{-8}$ for this study. Plots of φ with varying threshold θ and α are shown in Figure 6. We can see that φ

19

is a differentiable approximation to the step function with a step at θ. For a fixed θ, α increases the steepness of φ when making the transition from 0 to 1. For this study, we set $\alpha = 4$.

3.2.4. Balancing Reconstruction with Compression

To train `BCAE-VS`, we need to balance the reconstruction accuracy with compression. We do this by adjusting the reconstruction loss $\mathcal{L}_{\text{recon}}$ and compression loss $\mathcal{L}_{\text{comp}}$.

The reconstruction loss $\mathcal{L}_{\text{recon}}$ is the weighted sum of the segmentation loss $\mathcal{L}_{\text{seg}}$ and the regression loss $\mathcal{L}_{\text{reg}}$. We use focal loss [25] for segmentation since it is designed to deal with datasets with unbalanced classes (TPC data is sparse and hence has a high percentage of voxels in the class 0). We use mean absolute error (L_1) for regression following the convention in [15]. The reconstruction loss $\mathcal{L}_{\text{recon}}(x)$ is defined as $\lambda_{\text{seg}}\mathcal{L}_{\text{seg}}(x) + \mathcal{L}_{\text{reg}}(x)$ with λ_{seg} adjusted by the end of each epoch with the same method as discussed in [15, section 2.5]

Since `BCAE-VS` compresses by identifying key points, we want the average of p, denoted as μ, to be small, so that only the valuable signal voxels can get a high importance score. However, since there is no need for the average importance score to go arbitrarily small, we also set a lower bound l_{prob} so that the average importance will be penalized more lightly when it is close to l_{prob}, and will no longer be penalized if it goes below l_{prob}. Hence, the compression loss function of `BCAE-VS` is defined as

$$\mathcal{L}_{\text{comp}}\left(x, l_{\text{prob}}\right) = \begin{cases} \mu(x_s)\left(\mu(x_s) - l_{\text{prob}}\right) & \mu(x_s) > l_{\text{prob}} \\ 0 & \mu(x_s) \leq l_{\text{prob}} \end{cases}$$

20

The overall loss $\mathcal{L}(x)$ of `BCAE-VS` is defined as $\lambda_{\mathrm{comp}}\mathcal{L}_{\mathrm{comp}}\left(x_s, l_{\mathrm{prob}}\right) + \mathcal{L}_{\mathrm{recon}}(x)$. In this study, we set $l_{\mathrm{prob}} = .1$ and $\lambda_{\mathrm{comp}} = 30$.

4. Results

4.1. Reconstruction Accuracy

Table 1: Comparing compression algorithm with dense and sparse convolutions.

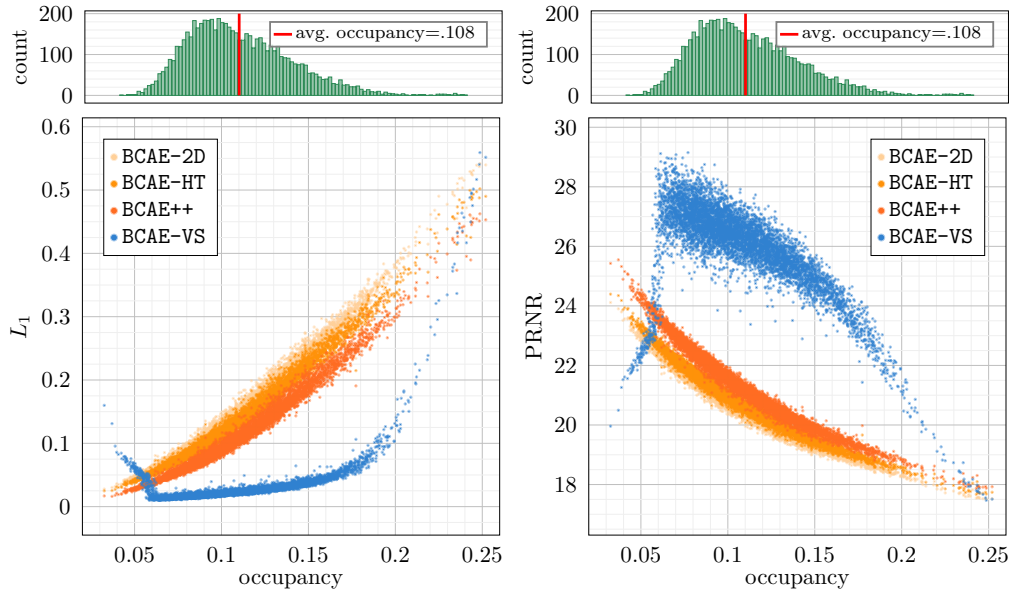| model	comp. ratio ↑	reconstruction performance					efficiency	
		$L_1 \downarrow$	$L_2 \downarrow$	PSNR ↑	recall ↑	precision ↑	encoder size	throughput ↑
`BCAE-2D`	31	.152	.862	20.6	.907	.906	169k	**9.6k**
`BCAE-HT (3D)`	31	.138	.781	20.8	.916	.915	9.8k	**9.6**k
`BCAE++ (3D)`	31	.112	.617	21.4	.936	.934	226k	3.2k
`BCAE-VS`	**34**	**.028**	**.089**	**26.0**	**.988**	**.996**	**382**	5.6k

Figure 8: **Reconstruction L_1 error (left) and peak signal-to-noise ratio (PSNR, right) as a function of occupancy for dense `BCAE` models.**
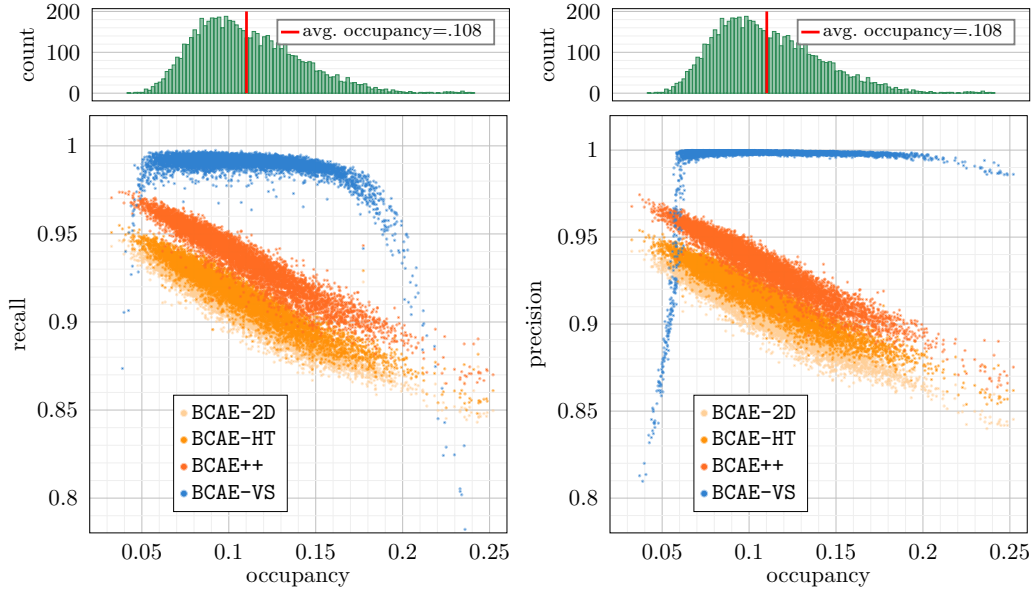
21

Figure 9: **Reconstruction recall (left) and precision (right) as a function of occupancy for dense BCAE models.**

Since there is no value below 6 in the input log ADC, we apply a zero-suppression at 6 to the reconstruction produced by BCAE-VS. The reason that we did not use the regression output transform approach (mapping all regression output to above 6) introduced in dense BCAEs [15] is because it makes the training of BCAE-VS unstable.

We measured the reconstruction accuracy in L_1, L_2, peak signal-to-noise ratio (PSNR), recall, and precision and listed the result in Table 1. We computed reconstruction from compressed data saved in half-precision (float16). Here, recall is defined as the fraction of signals that get a positive value in the prediction, and precision is defined as the fraction of true signals over all voxels that has a positive prediction. To compare the compression ratio of the BCAE-VS with those of the dense BCAE models, we use the convention
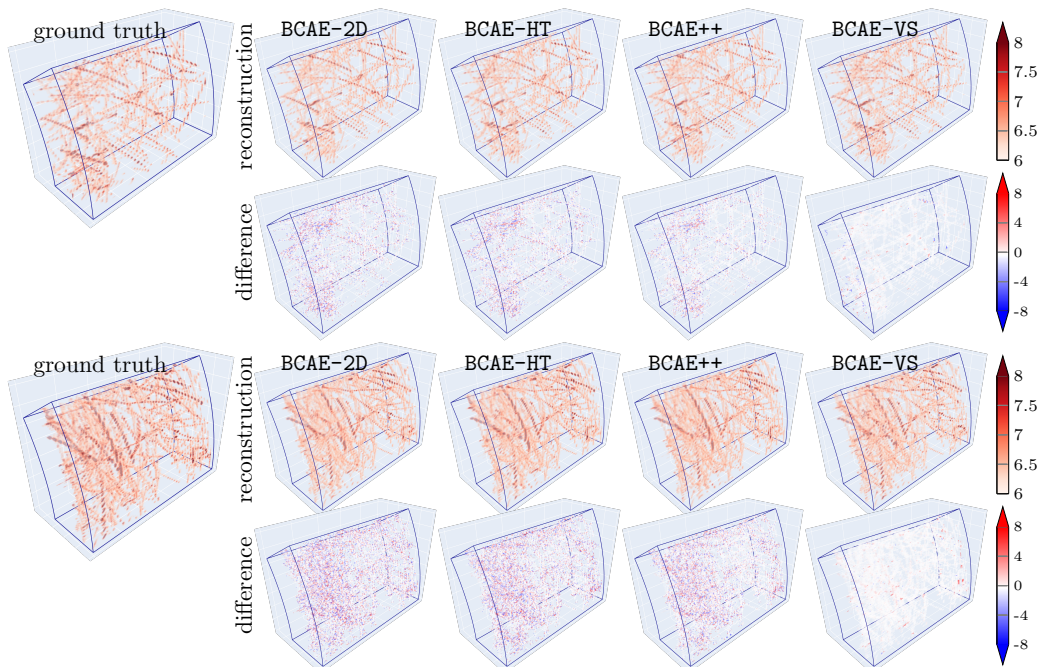
Figure 10: **Visualization of reconstruction performance for dense** `BCAE` **models.**

detailed in Section 4.2. The encoder size is measured by trainable parameters. The throughput is measured by the number of TPC wedges processed per second.

We also plot the dependence of reconstruction accuracy on occupancy in Figure 8 for L_1 and PSNR and in Figure 9 for recall and precision. We can observe that the reconstruction accuracy metrics (L_1, recall, and precision) of the dense `BCAE` models depend linearly on occupancy with a strong correlation. On the contrary, in a wide range of occupancy where the TPC wedges are the most populated, the sparse model `BCAE-VS`'s performance is correlated weakly with occupancy and maintains a superior performance. However, towards the two ends of the occupancy distribution, the `BCAE-VS` starts to fail. From Figure 9, we can observe that the failure of `BCAE-VS` is

driven by a drastic decline in recall for extremely high-occupancy input and by precision for low-occupancy ones.

In Figure 10, we compare BCAEs' reconstruction performance qualitatively on two TPC wedges. The difference is calculated by subtracting reconstruction from the ground truth. From the comparison, we can make two observations. First, dense BCAEs (BCAE-2D, BCAE-HT, BCAE++) have difficulty reconstructing a track at its correct location while BCAE-VS conserves the track location even in densely packed regions. This is evident with the cloud of blue and red dots and the lack thereof in the plot of difference. Second, dense BCAEs under-perform in input region with higher occupancy while BCAE-VS maintains accurate reconstruction over a wider range of occupancy.

4.2. Compression Ratio

The compression ratio of the algorithm depends on data precision and the format of storage of the input and the code.

On the input side, raw ADC values from TPC are collected as 10-bit integers. However, since most commonly used computing platforms cannot handle 10-bit integers, we consider input ADC values as 16-bits floats. For the input size, we follow the convention in the dense BCAEs works [15, 14] and define it as the size of the zero-padded regularly shaped tensors.

With respect to the precision of the code, although we train all models in full precision (float32), it is shown in [15] that the difference in accuracy between reconstruction from full-precision compressed data and those downcast to float16 is negligible. Similar observation can also be made for BCAE-VS according to Table 2. Hence, compressed data is saved in float16 format for all models.

24

Table 2: Reconstruction accuracy with full (float32) and half (float16) precision code.

precision	L_1	L_2	PSNR	recall	precision
half	.028394	.088652	26.000	.988447	.995573
full	.028415	.088818	25.996	.988419	.995569

Since a dense encoder output a code as a regularly shaped tensor, the compression ratio of a dense `BCAE` can be calculated directly as the ratio of the input size to the code size. However, since the code produced by the sparse encoder of `BCAE-VS` is a sparse tensor, to compute a compression ratio comparable to those of the dense models, we need the following conversion. Assume that the Coordinate List (`COO`) format is used for saving the output from the sparse encoder of `BCAE-VS`. We need to save the location and value of all entries in v whose corresponding value in p is larger than a (random) threshold. Since a TPC wedge has shape $(16, 192, 249)$, we need 4 bit to specify the index of in the first dimension, and 8 bits each for the second and last dimensions. Hence we need $(4 + 8 + 8) + 16 = 36$ bits to save one entry in v. Suppose the occupancy of the wedge is o and a fraction k of the entries in v will be retained, the compression ratio C for this wedge can be calculated using the following formula

$$C = \frac{16\text{bits} \times \text{input size}}{36\text{bits} \times \text{input size} \times o \times k} = \frac{4}{9ok} \tag{3}$$

Over the test split of the dataset, on average a fraction of .133 of the signal voxels is retained for each wedge. The averaged compression ratio is 33.9 with wedge-wise compression ratio calculated using Equation 3. The left panel of Figure 11 shows compression ratio and retention ratio as a function
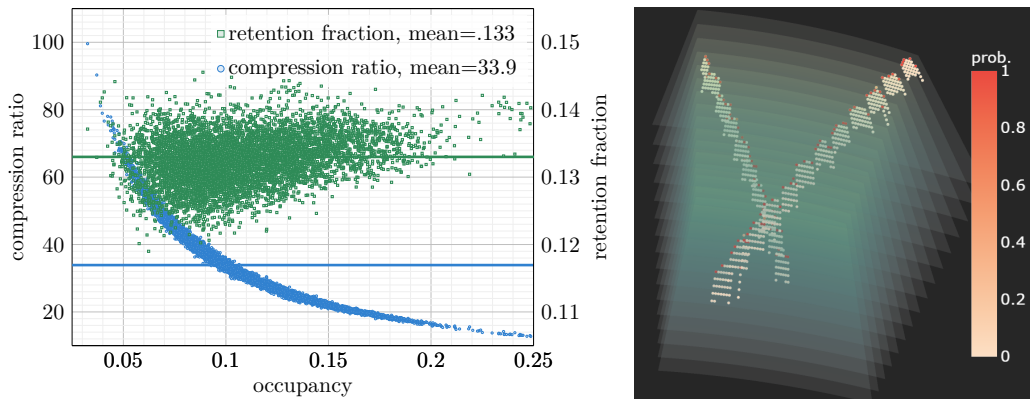
Figure 11: **Compression ratio, retention fraction (left), and importance assignment to the signal voxels (right).**

of occupancy. While the dependency of retention on occupancy is relatively weak, `BCAE-VS` tends to retain more signal voxels at higher occupancy. This behavior is desirable, as more voxels need to be preserved for accurate reconstruction when trajectories are closer together. The compression ratio, on the other hand, exhibits a clear inverse relationship to occupancy. These observations demonstrated `BCAE-VS`'s ability to dynamically adjust key-point identification and achieve a variable compression ratio.

We also visualize the importance score assignment by the encoder of `BCAE-VS` on isolated tracks in the right panel of Figure 11. We can see that the assignment is polarized – most of the probabilities are close to zero and only a small fraction of signal voxels along the boundary of a track are assigned with a high importance score.

4.3. Throughput

Unlike dense convolutions, the inference speed of sparse convolution depends on occupancy. As discussed in Section 3.2.1, lower occupancy leads to
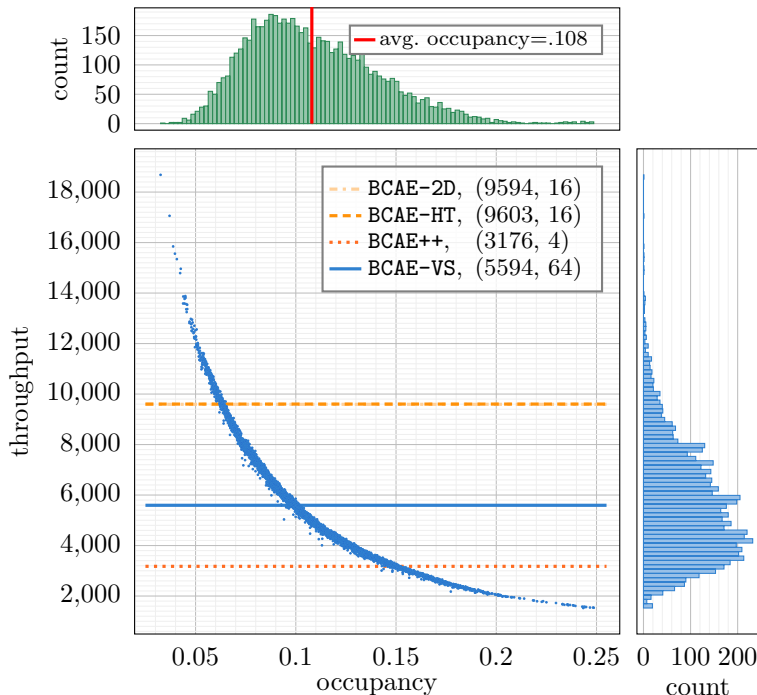
Figure 12: **Throughput comparison.** The lines of `BCAE-HT` and `BCAE-2D` overlap. The numbers in the parenthesis are the TPC wedges compressed per second and the batch size used to obtain the throughput.

fewer matrix multiplications. Therefore, in an occupancy regime where the speed gain reduced matrix multiplications outweigh the overhead of computing the kernel map, `BCAE-VS` may achieve lower compression latency. To test this hypothesis, we conducted a throughput study using a `NVIDIA` `RTX`™ `6000 ADA` graphic card with `driver 555.42.02` and `PyTorch 2.4.0` compiled with `CUDA 12.2`[3] and demonstrate the result in Figure 12. Here, throughput is measured as the number of TPC wedges compressed per second.

---

[3]A fix build of `MinkowskiEngine` for `CUDA 12.2` can be found at `https://github.com/NVIDIA/MinkowskiEngine/pull/567`

The throughput for each dense `BCAE` is averaged from 1000 batches with a warm-up of 10 batches. We evaluated throughput under the assumption that the input data is already stored in GPU memory. Figure 12 presents the peak throughput of each dense model, with the corresponding batch size that achieved the peak noted in the legend. All the dense `BCAE`s are compiled using `torch.compile` to optimize the inference speed.

For `BCAE-VS`, each test sample was repeated 64 times to generate the input. We assume the input batch of TPC wedges is already in GPU memory in a sparse-encoded format, ready for direct processing by the sparse network. This assumption is reasonable as the TPC data is collected and transferred in sparse encoding through the data acquisition pipeline.

The throughput is calculated on the test split of the dataset consisting of 6288 TPC wedges. Although `BCAE-VS` is slower than `BCAE-2D` and `BCAE-HT` on average, it is significantly faster in the lower occupancy regime. Moreover, sparse models can process sparsely encoded TPC data directly, eliminating the overhead of padding sparse encoding to a full tensor necessitated by a dense model. In many operational modes of collider tracking detectors, the occupancy can be significantly more sparse, e.g. on the order of 10^{-3}-10^{-2} for the TPC in the sPHENIX experiment during proton-proton collisions, which is much lower than in the high-pileup central Au+Au dataset studied in this work. The advantages of sparse convolution become increasingly pronounced in such conditions.

5. Conclusion

We introduced `BCAE-VS`, an algorithm designed to enhance the compression of sparse 3D TPC data from high-energy particle accelerators. `BCAE-VS` offers a variable compression ratio based on data occupancy, improving both compression efficiency and reconstruction accuracy. Our results show a 75% increase in reconstruction accuracy with a 10% higher average compression ratio compared to the leading `BCAE` model. By utilizing sparse convolution, `BCAE-VS` achieves an outstanding throughput within the operational occupancy range of sPHENIX. While the current model demonstrates promising performance, several limitations have been identified. We offer recommendations for future work to address these constraints and further enhance the model's capabilities.

- *Exact control of retention fraction:* Although hyperparameters such as $\mathcal{L}_{\mathrm{comp}}$ and l_{prob} (see Section 3.2.4) can influence `BCAE-VS`'s the retention fraction, we lack a direct control of it. A potential solution could involve thresholding by quantile of the importance score output p (see Section 3.2.1), allowing a fixed fraction of signals to be saved.

- *Performance at extreme occupancies:* While `BCAE-VS` performs well for typical occupancy levels in the dataset, it experiences a significant decrease in recall at high occupancy and in precision at low occupancy. For deployment, we need an algorithm that remains reliable even during extreme events.

- *Precision and quantization for throughput:* The sparse convolution library `MinkowskiEngine` does not support half-precision (float16) op-

erations. As demonstrated in [15], certain hardware can achieve substantial speedups with negligible performance loss using half-precision computation. Future work will explore more aggressive quantization schemes, such as int8, to further speed up inference.

- *Hardware support for sparse convolution:* Unlike dense convolution, sparse convolution engines are not commonly supported by innovative AI hardware accelerators. This poses additional challenges for deploying `BCAE-VS` on such hardware compared to dense convolutional models.

- *Downstream task:* Currently, the performance of `BCAE-VS` is evaluated with standard classification/regression metrics. However, being a compression algorithm of ADC readout, `BCAE-VS`'s performance needs to be tested on downstream tasks such as trajectory reconstruction and identification, which will be part of our future work.

- *Noisy TPC data from real experiment:* In this study, we used simulated collision data. However, the TPC data from real experiments will contain noises caused by, for example, common ground noise pickup. Hence, `BCAE-VS` needs to be retrained and tested with realistic noisy conditions in the actual TPC data and adjusted to incorporate noise-filtering mechanisms.

Acknowledgment

Appendix A. `BCAE-VS` neural network

The `BCAE-VS` network consists of a sparse encoder implemented with sparse convolution provided by the NVIDIA `MinkowskiEngine` library and two decoders implemented with normal dense convolution. The input to the neural network is one TPC wedge treated as a 4D array with 1 channel and 3 spatial dimensions.

The sparse encoder has five 3D convolution layers, all with 2 output channels, kernel size 3, stride 1, and no padding. The dilation parameters of the convolutions are $1, 2, 4, 2, 1$. There is a rectified linear unit (`ReLU`) activation between two successive convolutional layers. The output activation is `Sigmoid`.

The two decoders share the same structure. Each one of them has eight (dense) convolutional blocks with one convolution (kernel size 3, padding 1, stride 1, dilation 1) followed by a leaky `ReLU` with negative slope .1. The number of output channels are $(16, 16, 16, 8, 8, 8, 4, 2)$. A final 1×1 convolution maps the number of channels back to 1. The regression decoder D_{reg} has no output activation while the segmentation decoder D_{seg} has `Sigmoid` as output activation.

No normalization is used in the `BCAE-VS` model.

Appendix B. `BCAE-VS` training

The training is done for 100 epochs with a batch size of 4 and 2000 batches per epoch. For optimization, we used the Adam optimizer with decoupled weight decay (`AdamW`) with an initial learning rate 0.001, $(\beta_1, \beta_2) = (0.9, 0.999)$, and weight decay 0.01. We kept the learning rate as initialized for the first 20 epochs and decreased it to the 95% of the previous value every 20 epochs thereafter.

References

[1] L. Evans, P. Bryant, LHC machine 3 (8) S08001. `doi:10.1088/1748-0221/3/08/S08001`.
URL `https://dx.doi.org/10.1088/1748-0221/3/08/S08001`

[2] sPHENIX Collaboration, Technical design report: sphenix experiment at rhic (2019).
URL `https://indico.bnl.gov/event/5905/`

[3] H. J. Hilke, Time Projection Chambers, Rep. Prog. Phys. 73 (11) (2010) 116201. `doi:10.1088/0034-4885/73/11/116201`.
URL `https://cds.cern.ch/record/1302071`

[4] sPHENIX Collaboration, sphenix 2023 beam use proposal (2023).
URL `https://indico.bnl.gov/event/20373/`

[5] J. C. Bernauer, et al., Scientific computing plan for the ECCE detector at the Electron Ion Collider, Nucl. Instrum. Meth. A 1047 (2023) 167859. `arXiv:2205.08607, doi:10.1016/j.nima.2022.167859`.

[6] R. Abdul Khalek, et al., Science Requirements and Detector Concepts for the Electron-Ion Collider: EIC Yellow Report, Nucl. Phys. A 1026 (2022) 122447. `arXiv:2103.05419, doi:10.1016/j.nuclphysa.2022.122447`.

[7] D. Rohr, Gpu-based reconstruction and data compression at alice during lhc run 3, in: EPJ Web of Conferences, Vol. 245, EDP Sciences, 2020, p. 10005.

[8] S. Di, F. Cappello, Fast error-bounded lossy HPC data compression with SZ, in: 2016 IEEE International Parallel and Distributed Processing Symposium (IPDPS), pp. 730–739, ISSN: 1530-2075. `doi:10.1109/IPDPS.2016.11`.

[9] D. Tao, S. Di, Z. Chen, F. Cappello, Significantly improving lossy compression for scientific data sets based on multidimensional prediction and error-controlled quantization, in: 2017 IEEE International Parallel and Distributed Processing Symposium (IPDPS), pp. 1129–1139, ISSN: 1530-2075. `doi:10.1109/IPDPS.2017.115`.

[10] Y. Liu, S. Di, K. Zhao, S. Jin, C. Wang, K. Chard, D. Tao, I. Foster, F. Cappello, Optimizing error-bounded lossy compression for scientific data with diverse constraints 33 (12) 4440–4457, conference Name: IEEE Transactions on Parallel and Distributed Systems. `doi:10.1109/TPDS.2022.3194695`.

[11] P. Lindstrom, Fixed-rate compressed floating-point arrays 20 (12) 2674–

2683, conference Name: IEEE Transactions on Visualization and Computer Graphics. `doi:10.1109/TVCG.2014.2346458`.

[12] M. Ainsworth, O. Tugluk, B. Whitney, S. Klasky, Multilevel techniques for compression and reduction of scientific data—the multivariate case 41 (2) A1278–A1303, publisher: Society for Industrial and Applied Mathematics. `doi:10.1137/18M1166651`.
URL `https://epubs.siam.org/doi/10.1137/18M1166651`

[13] X. Liang, B. Whitney, J. Chen, L. Wan, Q. Liu, D. Tao, J. Kress, D. Pugmire, M. Wolf, N. Podhorszki, S. Klasky, MGARD+: Optimizing multilevel methods for error-bounded scientific data reduction 71 (7) 1522–1536, conference Name: IEEE Transactions on Computers. `doi: 10.1109/TC.2021.3092201`.

[14] Y. Huang, Y. Ren, S. Yoo, J. Huang, Efficient data compression for 3d sparse tpc via bicephalous convolutional autoencoder, in: 2021 20th IEEE International Conference on Machine Learning and Applications (ICMLA), 2021, pp. 1094–1099. `doi:10.1109/ICMLA52953.2021. 00179`.

[15] Y. Huang, Y. Ren, S. Yoo, J. Huang, Fast 2d bicephalous convolutional autoencoder for compressing 3d time projection chamber data, in: Proceedings of the SC'23 Workshops of The International Conference on High Performance Computing, Network, Storage, and Analysis, 2023, pp. 298–305.

[16] D. Avola, L. Cinque, A. Fagioli, G. L. Foresti, A. Fragomeni, D. Pan-

none, 3d hand pose and shape estimation from rgb images for keypoint-based hand gesture recognition, Pattern Recognition 129 (2022) 108762.

[17] Y. Lin, W. Chi, W. Sun, S. Liu, D. Fan, Human action recognition algorithm based on improved resnet and skeletal keypoints in single image, Mathematical Problems in Engineering 2020 (1) (2020) 6954174.

[18] Y. You, Y. Lou, C. Li, Z. Cheng, L. Li, L. Ma, C. Lu, W. Wang, Keypointnet: A large-scale 3d keypoint dataset aggregated from numerous human annotations, in: Proceedings of the IEEE/CVF Conference on Computer Vision and Pattern Recognition, 2020, pp. 13647–13656.

[19] O. Moskvyak, F. Maire, F. Dayoub, M. Baktashmotlagh, Keypoint-aligned embeddings for image retrieval and re-identification, in: Proceedings of the IEEE/CVF winter conference on applications of computer vision, 2021, pp. 676–685.

[20] X.-N. Wang, M. Gyulassy, HIJING: A Monte Carlo model for multiple jet production in p p, p A and A A collisions, Phys. Rev. D 44 (1991) 3501–3516. `doi:10.1103/PhysRevD.44.3501`.

[21] J. Allison, et al., Recent developments in Geant4, Nucl. Instrum. Meth. A 835 (2016) 186–225. `doi:10.1016/j.nima.2016.06.125`.

[22] sPHENIX, sphenix software repositories https://github.com/sphenix-collaboration (2019).
URL `https://github.com/sPHENIX-Collaboration`

[23] Y. Alanazi, N. Sato, T. Liu, W. Melnitchouk, M. P. Kuchera,

E. Pritchard, M. Robertson, R. Strauss, L. Velasco, Y. Li, Simulation of electron-proton scattering events by a feature-augmented and transformed generative adversarial network (fat-gan), arXiv preprint arXiv:2001.11103 (2020).

[24] B. Hashemi, N. Amin, K. Datta, D. Olivito, M. Pierini, Lhc analysis-specific datasets with generative adversarial networks, arXiv e-prints (2019) arXiv–1901.

[25] T.-Y. Lin, P. Goyal, R. Girshick, K. He, P. Dollár, Focal loss for dense object detection, in: Proceedings of the IEEE international conference on computer vision, 2017, pp. 2980–2988.